Transmission Electron Microscopy and High-Resolution Electron Microscopy Investigation of the Microstructure of an YNi_2B_2C Thin Film

G. H. Cao* and W. Skrotzki†

Institute of Structural Physics, TU Dresden, D-01062 Dresden, Germany

P. Simon

Max Planck Institute for Chemical Physics of Solids, D-01187 Dresden, Germany

S. C. Wimbush§ and B. Holzapfel

IFW Dresden, P.O. Box 270016, D-01171 Dresden, Germany

Received January 3, 2005. Revised Manuscript Received April 15, 2005

An YNi_2B_2C thin film grown on a MgO(001) substrate by pulsed laser deposition has been investigated by transmission electron microscopy (TEM) and high-resolution electron microscopy (HREM). Plan-view TEM analyses show that the film consists of isolated rectangular YNi_2B_2C grains distributed within a second phase. This phase was identified as monoclinic $Y_2Ni_{15}B_6$ with lattice parameters $a = 1.42$ nm, $b = 1.07$ nm, $c = 0.96$ nm, and $\beta = 95°$. Within the YNi_2B_2C grains, a hexagonal $Y_{0.915}Ni_{4.12}B$ phase with lattice parameters $a = 1.49$ nm and $c = 0.69$ nm is intergrown with a cubic Y_2O_3 phase with lattice parameter $a = 1.06$ nm. The orientation relationships between YNi_2B_2C, Y_2O_3, and $Y_{0.915}Ni_{4.12}B$ are analyzed, and the mechanisms of phase formation are discussed.

1. Introduction

Quaternary rare earth transition metal borocarbides RT_2B_2C (R = rare earth, T = transition metal) have aroused great interest due to the interplay of magnetic ordering and superconductivity within the materials. (For a review, see, for example, ref 1) The tetragonal compound YNi_2B_2C (space group No. 139, $I4/mmm$, $a = 0.353$ nm, $c = 1.054$ nm), possessing no magnetic order, exhibits a fairly high T_c value of around 15 K. A study of the Y-based compound is therefore a prerequisite for the understanding of its magnetic counterparts, since it is free from the complications introduced by the presence of magnetic ordering, and ideal for investigating the origin of superconductivity in the borocarbides.[2] With high-quality samples available in bulk polycrystalline form and as single crystals, considerable research on these compounds has been reported. On the other hand, high-quality thin films are useful both for the study of particular physical properties and for the exploration of potential applications.[3] YNi_2B_2C thin films have been prepared by several groups, using both sputtering[4,5] and pulsed laser deposition.[3,6] Most of the investigations into YNi_2B_2C thin films have focused on film preparation and characterization; however, microstructural investigations by transmission electron microscopy (TEM) are still limited. In a previous work,[7] TEM and high-resolution electron microscopy (HREM) investigations of an YNi_2B_2C thin film on a Y_2O_3-buffered MgO(001) substrate were reported, showing the orientation relationships between the Y_2O_3 buffer layer, MgO substrate, and YNi_2B_2C film. Moreover, a hexagonal precipitate, $Y_{0.915}Ni_{4.12}B$, was found at the interface between YNi_2B_2C and Y_2O_3. Reibold et al.[8] showed that an interlayer consisting of Y_2O_3, Ni_3B, and YNi_4B exists in the cross-sectional sample of YNi_2B_2C deposited on MgO. Recently, the present authors[9] reported on plan-view TEM investigations of YNi_2B_2C deposited on MgO(001). It was shown that the YNi_2B_2C film consisted of isolated rectangular grains distributed within a monoclinic $Y_2Ni_{15}B_6$ phase. It is the aim of this work to present new results obtained by plan-

* To whom correspondence should be addressed. Current address: 206 Metals Development, Ames Laboratory, Iowa State University, Ames, IA 50011-3020. Fax: (515) 294 8727. E-mail: ghcao@ameslab.gov.

† E-mail: werner.skrotzki@physik.tu-dresden.de.

§ Current address: National Institute for Materials Science, International Center for Young Scientists, 1-1 Namiki, Tsukuba, Ibaraki 305-0044, Japan.

(1) Müller, K.-H.; Narozhnyi, V. N. *Rep. Prog. Phys.* **2001**, *64*, 943.
(2) Andreone, A.; Gassinese, A.; Gianni, L.; Iavarone, M.; Palomba, F.; Vaglio, R. *Phys. Rev. B* **2001**, *64*, 100505.
(3) Grassano, G.; Marre, D.; Pallecchi, I.; Ricce, F.; Ferdeghini, C. *Supercond. Sci. Technol.* **2001**, *14*, 117.
(4) Arisawa, S.; Hatano, T.; Hirata, K.; Mochiku, T.; Kitaguchi, H.; Fujii, H.; Kumakura, H.; Kadowaki, K.; Nakamura, K.; Togano, K. *Appl. Phys. Lett.* **1994**, *65*, 1299.
(5) Andreone, A.; Iavarone, M.; Vaglio, R.; Manini, P.; Cogliati, E. *Appl. Phys. Lett.* **1996**, *69*, 118.
(6) Wimbush, S. C.; Häse, K.; Schultz, L.; Holzapfel, B. *J. Phys.: Condens. Matter* **2001**, *13*, L355.
(7) Cao, G. H.; Simon, P.; Krämer, U.; Wimbush, S. C.; Holzapfel, B. *Chem. Mater.* **2004**, *16*, 842.
(8) Reibold, M.; Wimbush, S. C.; Holzapfel, B.; Krämer, U. *J. Alloys Compd.* **2002**, *347*, 24.
(9) Cao, G. H.; Simon, P.; Skrotzki, W.; Wimbush, S. C.; Holzapfel, B. *Appl. Phys. A*, in press.

10.1021/cm050006t CCC: $30.25
Published on Web 05/28/2005

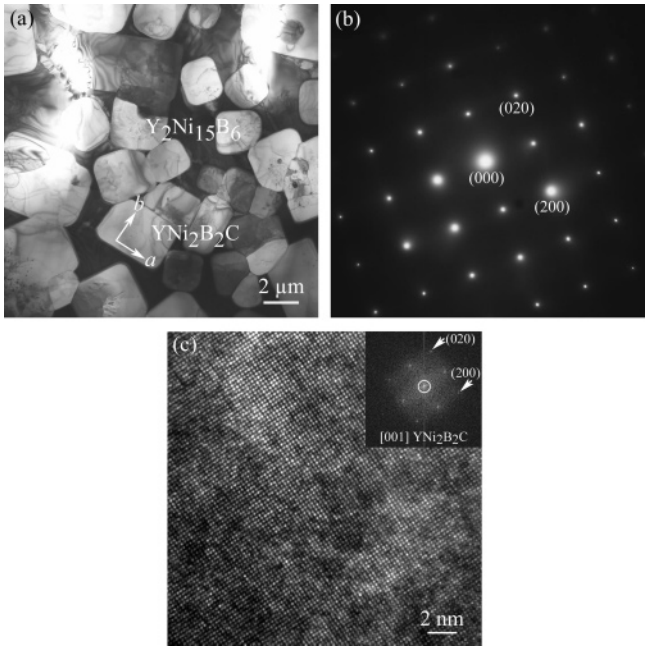

Figure 1. (a) Bright field plan-view TEM image showing the rectangular grain distribution of the YNi_2B_2C film. (b) SAED pattern and (c) HREM image with FFT inset of an YNi_2B_2C grain along the [001] zone axis.

view TEM and HREM of YNi_2B_2C deposited on MgO(001). The study provides an improved understanding of the growth processes of YNi_2B_2C thin films.

2. Experimental Section

An YNi_2B_2C thin film was prepared by pulsed laser deposition in an ultrahigh vacuum (base pressure $<10^{-9}$ mbar) chamber from a stoichiometric polycrystalline YNi_2B_2C target synthesized by arc melting. The target was ablated using a KrF excimer laser (wavelength 248 nm) while the temperature of the MgO(001) substrate was maintained at 950 °C. The incident energy density on the target was $\sim$5 J cm^{-2} at a laser pulse repetition rate of 30 Hz. As a result of the extraordinarily high deposition temperature, the sample peeled cleanly off of the substrate upon removal from the deposition chamber. A plan-view TEM specimen was prepared from the peeled-off film by Ar ion milling. TEM bright field imaging, selected area electron diffraction (SAED), and energy-dispersive X-ray (EDX) analyses were performed using a Philips CM200 electron microscope equipped with a LaB_6 electron source and operated at an acceleration voltage of 200 kV. The HREM images were taken in a Philips CM200 FEGST-Lorentz electron microscope equipped with a field emission gun, also operated at 200 kV.

3. Results and Discussion

Figure 1a is a bright field TEM image showing a distribution of isolated rectangular YNi_2B_2C grains of different sizes. A preferred orientation of the grains is evident, with the straight faces of the grains lying at around 45° to the edges of the image. Figure 1b is the SAED pattern of one grain showing it along the [001] zone axis. SAED indicates that the *a*-axes of the YNi_2B_2C unit cell are aligned parallel to the faces of the grains. Figure 1c shows the HREM image of an YNi_2B_2C grain. The inset is the fast Fourier transform (FFT) of this image, which is consistent with the SAED pattern of Figure 1b.

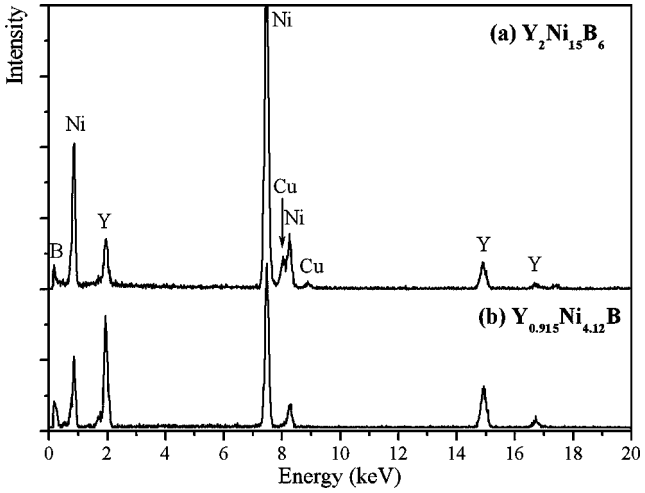

Figure 2. EDX spectra of (a) $Y_2Ni_{15}B_6$ and (b) $Y_{0.915}Ni_{4.12}B$ phases. Cu peaks originate from the TEM specimen support grid.

The EDX spectrum of the intergranular phase (Figure 2a) indicates a Ni-rich compound comprising the elements Ni, Y, and B, with an Y:Ni ratio close to 1:8. The sample was tilted through a wide range of angles to obtain SAED patterns suitable for determination of its crystal lattice. From these patterns (Figure 3a−c), it is deduced that the phase has a monoclinic lattice with lattice parameters $a = 1.42$ nm, $b = 1.07$ nm, $c = 0.96$ nm, and $\beta = 95°$. Kuz'ma et al.[10] reported that the Y−Ni−B system can form a number of ternary borides, including a monoclinic (space group No. 14, $P2_1/c$) $Y_2Ni_{15}B_6$ phase with lattice parameters $a = 1.4224$ nm, $b = 1.0679$ nm, $c = 0.9577$ nm, and $\beta = 94.37°$. A corresponding monoclinic phase, $Ho_2Ni_{15}B_6$, has also been reported in the Ho−Ni−B system,[11] having lattice parameters $a = 1.4223$ nm, $b = 1.0672$ nm, $c = 0.9582$ nm, and $\beta = 94.2°$. Therefore, on the basis of its crystal lattice, lattice parameters, and chemical composition, it is concluded that this phase is $Y_2Ni_{15}B_6$, as has been reported previously.[9] Figure 3d shows the HREM image of an $Y_2Ni_{15}B_6$ grain; the inset is the FFT of this image, which is in agreement with the SAED pattern of Figure 3b. Figure 3e is the HREM image of the interface region between YNi_2B_2C and $Y_2Ni_{15}B_6$. The interface shown is parallel to (100) of YNi_2B_2C. The FFTs of parts of the image corresponding to YNi_2B_2C, $Y_2Ni_{15}B_6$, and the interface region of YNi_2B_2C and $Y_2Ni_{15}B_6$ are shown in Figure 3f−h. Figure 3h indicates that no unique orientation relationship exists between $Y_2Ni_{15}B_6$ and YNi_2B_2C.

Figure 4a is a bright field TEM image showing some precipitates formed within the YNi_2B_2C grains. With higher magnification, Figure 4b, it is seen that two precipitates (B, C) coexist within the same YNi_2B_2C grain (A). Electron diffraction reveals that the YNi_2B_2C grain shown has the same SAED pattern as that of Figure 1b. Figure 4c is the SAED pattern of the precipitate marked C, indicating that it is Y_2O_3 (space group No. 206, *I*a3) with lattice parameter $a = 1.06$ nm. Figure 4d is the superposition of the SAED patterns of YNi_2B_2C (grain A) and Y_2O_3 (grain C) revealing

(10) Gubich, I. B.; Kuz'ma, Y. B. *Inorg. Mater.* **1991**, *27*, 916.
(11) Glowiak, T.; Orishin, S. V.; Gubich, I. B.; Chaban, N. F.; Kuz'ma, Y. B. *Sov. Phys.*—Crystallogr. (SPHCA) **1989**, *34*, 602.

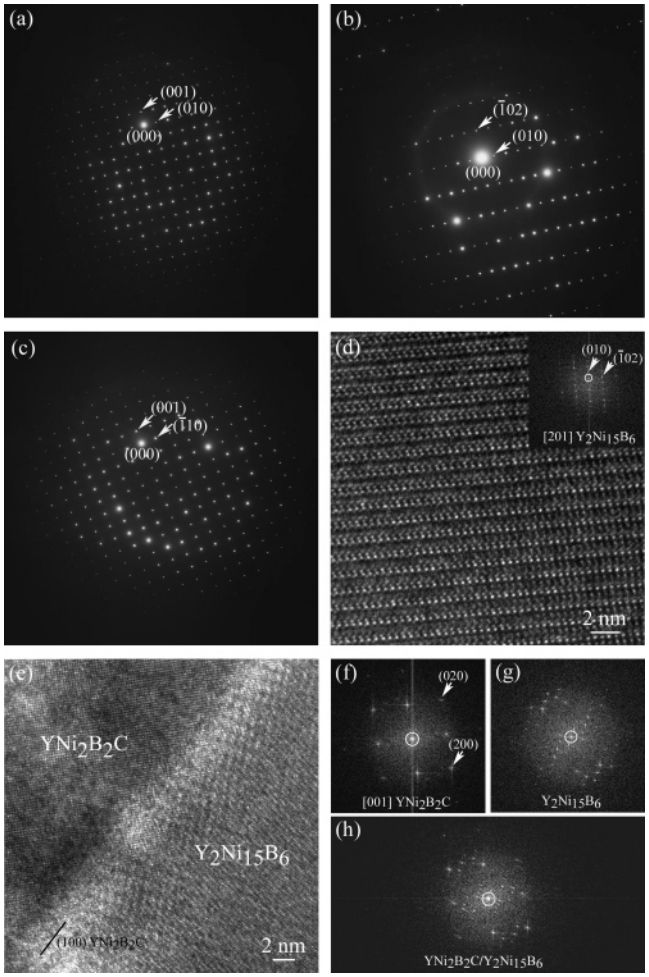

Figure 3. SAED patterns of $Y_2Ni_{15}B_6$ along the (a) [100], (b) [201], and (c) [110] zone axes. (d) HREM image with FFT inset of [201]-oriented $Y_2Ni_{15}B_6$. (e) HREM image of the interface region between YNi_2B_2C and $Y_2Ni_{15}B_6$. FFTs of (f) [001]-oriented YNi_2B_2C, (g) $Y_2Ni_{15}B_6$, and (h) the interface of YNi_2B_2C and $Y_2Ni_{15}B_6$.

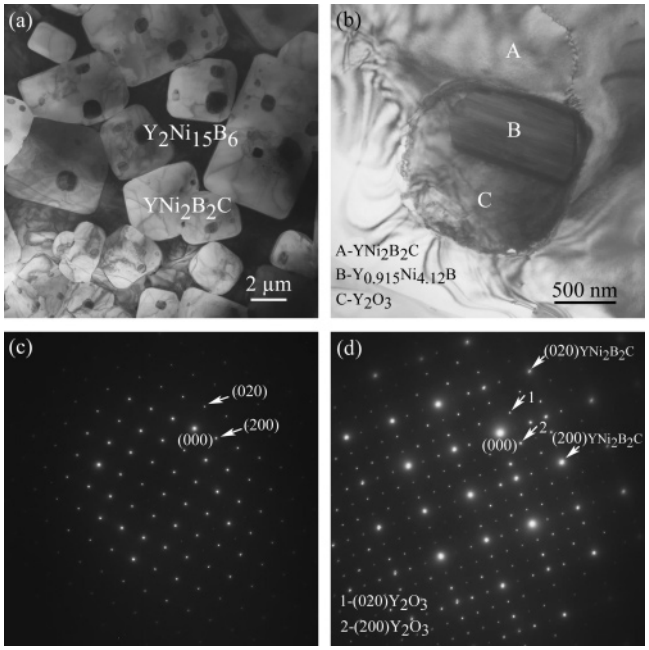

Figure 4. (a) Bright field plan-view TEM image showing precipitate formation inside rectangular YNi_2B_2C grains. (b) High-magnification view of one YNi_2B_2C grain containing two types of precipitates. (c) SAED pattern of Y_2O_3 (grain C) along the [001] zone axis. (d) SAED patterns of Y_2O_3 (grain C) with YNi_2B_2C (grain A).

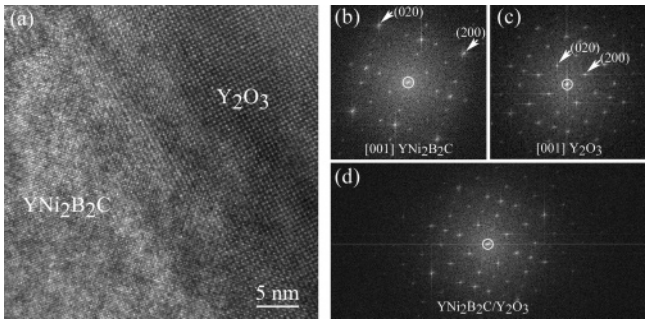

Figure 5. (a) HREM image of the interface region between YNi_2B_2C and Y_2O_3. FFTs of (b) [001]-oriented YNi_2B_2C, (c)-[001] oriented Y_2O_3, and (d) the interface between YNi_2B_2C and Y_2O_3.

the orientation relationship $YNi_2B_2C(100)[001]||Y_2O_3(100)$-[001]. Figure 5a shows the HREM image of the interface region between YNi_2B_2C and Y_2O_3. The interface is not clearly defined. The FFTs of parts of the image corresponding to YNi_2B_2C, Y_2O_3, and the interface region of YNi_2B_2C and Y_2O_3 are shown in Figure 5b−d. The crystallographic orientations of YNi_2B_2C and Y_2O_3 deduced from Figure 5d are in good agreement with those obtained from the SAED patterns shown in Figure 4d.

Figure 6a is the SAED pattern of the precipitate marked B, which is incompatible with the patterns of compounds such as YNi_4B, YNi_2B_2C, and the above $Y_2Ni_{15}B_6$. The EDX spectrum of this phase (Figure 2b) again indicates a Ni-rich compound comprising the elements Ni, Y, and B, this time with an Y:Ni ratio close to 1:4, lower than that in Figure 2a. To determine its crystal lattice, the sample was tilted and a series of diffraction patterns were recorded (Figure 6b,c). Indexing shows that this phase has a hexagonal crystal structure with lattice parameters $a = 1.49$ nm and $c = 0.69$ nm. YNi_4B is one compound in the Y−Ni−B system having a hexagonal structure (space group No. 191, *P*6/*mmm*), with a much shorter a lattice parameter, $a = 0.4977(4)$ nm and $c = 0.6942(5)$ nm.[12] Kuz'ma et al.[13] reported that the Y−Ni−B system can form a number of ternary borides, including a hexagonal "YNi_4B" phase with lattice parameters $a = 1.489(5)$ nm and $c = 0.691(2)$ nm, in agreement with our observation. They considered this YNi_4B to be a superstructure of the other. However, no detailed information on the atomic coordinates is available. Belger et al.[14] reported the full structural characterization of the phase $Y_{0.915}Ni_{4.12}B$, having similar lattice parameters, also considering this to be a superstructure of YNi_4B. Therefore, on the basis of its crystal lattice, lattice parameters, and chemical composition, it is concluded that this phase is $Y_{0.915}Ni_{4.12}B$. Figure 6d shows the HREM image of the $Y_{0.915}Ni_{4.12}B$ grain. The inset is the FFT of this image, which is consistent with the SAED pattern of Figure 6a. Parts e and f of Figure 6 are the SAED patterns of $Y_{0.915}Ni_{4.12}B$ (grain B) with Y_2O_3 (grain C) and YNi_2B_2C (grain A),

(12) Niihara, K.; Katayama, Y.; Yajima, S. *Chem. Lett.* **1973**, *6*, 613.
(13) Kuz'ma, Y. B.; Khaburskaya, M. P. *Inorg. Mater.* **1975**, *11*, 1625.
(14) Belger, A.; Zahn, G.; Wehner, B.; Paufler, P.; Graw, G.; Behr, G. *J. Alloys Compd.* **1999**, *26*, 283.

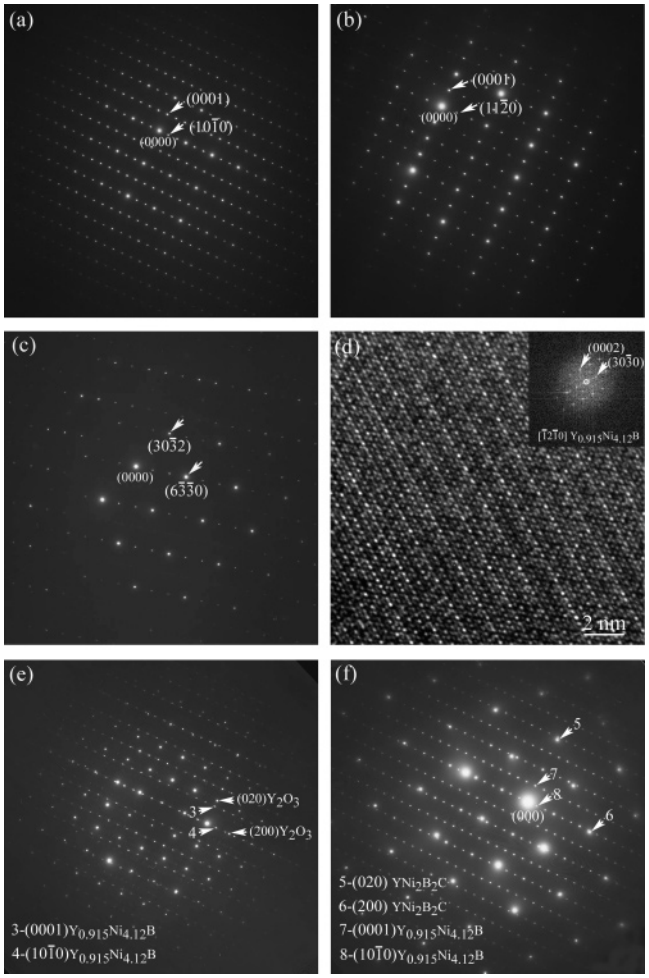

Figure 6. SAED patterns of the $Y_{0.915}Ni_{4.12}B$ precipitate (grain B) along the (a) [$\bar{1}$2$\bar{1}$0], (b) [1$\bar{1}$00], and (c) [0$\bar{2}$23] zone axes. (d) HREM image with FFT inset of [$\bar{1}$2$\bar{1}$0]-oriented $Y_{0.915}Ni_{4.12}B$. SAED patterns of the $Y_{0.915}Ni_{4.12}B$ precipitate with (e) Y_2O_3 and (f) YNi_2B_2C.

yielding the orientation relationships $Y_{0.915}Ni_{4.12}B$ (10$\bar{1}$0)-[$\bar{1}$2$\bar{1}$0]||Y_2O_3(100)[001] and $Y_{0.915}Ni_{4.12}B$ (10$\bar{1}$0)[$\bar{1}$2$\bar{1}$0]|| YNi_2B_2C(100)[001].

It is interesting to note that such a boride, $Y_{0.915}Ni_{4.12}B$, has been observed[7] bordering at the interface between YNi_2B_2C and Y_2O_3 in a cross-sectional sample of YNi_2B_2C deposited on a Y_2O_3-buffered MgO substrate. However, no specific orientation relationships of $Y_{0.915}Ni_{4.12}B$ with the YNi_2B_2C film and Y_2O_3 buffer layer were found.

Figures 7a and 8a show the HREM images of the interface regions between $Y_{0.915}Ni_{4.12}B$ and Y_2O_3 and YNi_2B_2C. The interface orientations are not clearly defined. The FFTs of parts of the images corresponding to $Y_{0.915}Ni_{4.12}B$, YNi_2B_2C, Y_2O_3, and the interface regions are shown in Figures 7b−d and 8b−d. The crystallographic orientations of $Y_{0.915}Ni_{4.12}B$ with respect to Y_2O_3 and YNi_2B_2C observed from the FFTs in Figures 7d and 8d are again in good agreement with those obtained from the SAED patterns of Figure 6e,f.

The preceding observations show that rectangular YNi_2B_2C grains exist distributed in a $Y_2Ni_{15}B_6$ matrix, and that the precipitates $Y_{0.915}Ni_{4.12}B$ and Y_2O_3 coexist within the YNi_2B_2C grains. Since the film deposition takes place in ultrahigh vacuum, it is proposed that the oxygen for Y_2O_3 formation

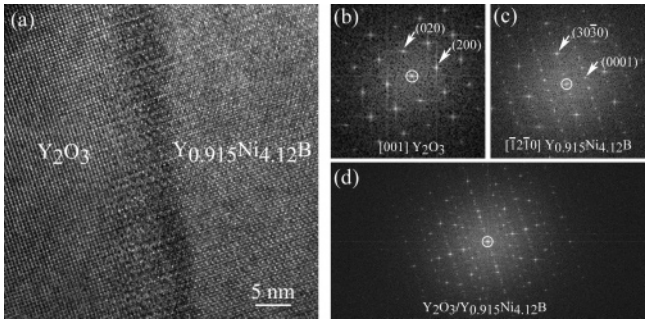

Figure 7. (a) HREM image of the interface region between Y_2O_3 and $Y_{0.915}Ni_{4.12}B$. FFTs of (b) [001]-oriented Y_2O_3, (c) [$\bar{1}$2$\bar{1}$0]-oriented $Y_{0.915}Ni_{4.12}B$, and (d) the interface between Y_2O_3 and $Y_{0.915}Ni_{4.12}B$.

is released from the MgO substrate. The free energy for the formation of Y_2O_3 (−1815 kJ/mol) is smaller than that of B_2O_3 (−1193 kJ/mol), CO_2 (−384 kJ/mol), and NiO (−212 kJ/mol),[15] so the formation of Y_2O_3 is thermodynamically most favorable. Due to the formation of Y_2O_3, the resultant Y deficiency leads to the precipitation of low-Y-content precipitates such as $Y_{0.915}Ni_{4.12}B$ and $Y_2Ni_{15}B_6$. Reibold et al.[8] observed an unidentified phase during HREM studies on a cross-sectional sample of YNi_2B_2C grown on MgO(001), besides Y_2O_3 mixed with Ni_3B and YNi_4B. Comparing the results (Figure 3) of the present work with the FFTs of the HREM images of the unknown phase shown in Figure 8 of ref 8, it is possible to consistently identify this phase as $Y_2Ni_{15}B_6$.

In the case of $YNi_2B_2C(100)[001]||Y_2O_3(100)[001]$, the c-axis lattice mismatch is $\delta = (c_{YNi_2B_2C} - c_{Y_2O_3})/c_{Y_2O_3} \approx -0.6\%$. In the case of $Y_{0.915}Ni_{4.12}B(10\bar{1}0)[\bar{1}2\bar{1}0]||Y_2O_3(100)[001]$, it may be supposed that two unit cells of $Y_{0.915}Ni_{4.12}B$ are superimposed on three unit cells of Y_2O_3. The corresponding lattice mismatch is $\delta = (2a_{Y_{0.915}Ni_{4.12}B} - 3c_{Y_2O_3})/3c_{Y_2O_3} \approx -6\%$. For $Y_{0.915}Ni_{4.12}B(10\bar{1}0)[\bar{1}2\bar{1}0]||YNi_2B_2C(100)[001]$, supposing two unit cells of $Y_{0.915}Ni_{4.12}B$ are superimposed on three unit cells of YNi_2B_2C, the corresponding lattice mismatch is $\delta = (2a_{Y_{0.915}Ni_{4.12}B} - 3c_{YNi_2B_2C})/3c_{YNi_2B_2C} \approx -6\%$. In all three cases the lattice mismatch is quite low, indicating low internal stresses in YNi_2B_2C, Y_2O_3, and $Y_{0.915}Ni_{4.12}B$. This may explain why Y_2O_3 and $Y_{0.915}Ni_{4.12}B$ precipitates form together in an YNi_2B_2C grain. Ways to eliminate these precipitates should be further investigated.

4. Conclusions

Plan-view TEM and HREM observations of an YNi_2B_2C thin film deposited on a MgO(001) substrate have revealed three impurity phases: Y_2O_3, $Y_2Ni_{15}B_6$, and $Y_{0.915}Ni_{4.12}B$. The monoclinic $Y_2Ni_{15}B_6$ phase is distributed between rectangular YNi_2B_2C grains. The hexagonal $Y_{0.915}Ni_{4.12}B$ phase coexists with a cubic Y_2O_3 phase within the rectangular YNi_2B_2C grains. The orientation relationships of YNi_2B_2C with Y_2O_3 and $Y_{0.915}Ni_{4.12}B$ and of $Y_{0.915}Ni_{4.12}B$ with Y_2O_3 are $YNi_2B_2C(100)[001]||Y_2O_3(100)[001]$, $YNi_2B_2C(100)[001]||$

(15) Dean, J. A. *Lange's Handbook of Chemistry*; McGraw-Hill Book Co.: New York, 1985.

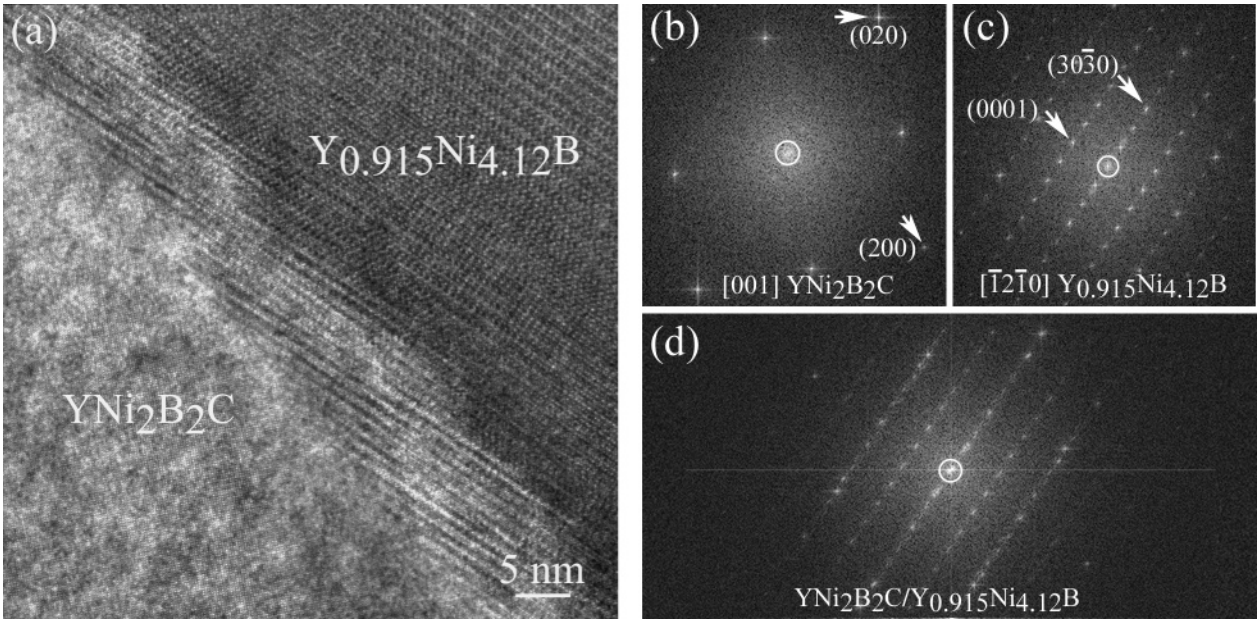

Figure 8. (a) HREM image of the interface region between YNi_2B_2C and $Y_{0.915}Ni_{4.12}B$. FFTs of (b) [001]-oriented YNi_2B_2C, (c) $[\bar{1}2\bar{1}0]$-oriented $Y_{0.915}Ni_{4.12}B$, and (d) the interface between YNi_2B_2C and $Y_{0.915}Ni_{4.12}B$.

$Y_{0.915}Ni_{4.12}B(10\bar{1}0)[\bar{1}2\bar{1}0]$, and $Y_{0.915}Ni_{4.12}B(10\bar{1}0)[\bar{1}2\bar{1}0]||Y_2O_3$-(100)[001]. These orientation relationships yield a small lattice mismatch. The impurity phases formed result from deviations from stoichiometry which are due to Y_2O_3 formation, leading to a depletion of Y. As the continuous Y_2O_3 layer usually found at the MgO interface has not been observed in the film, it may be concluded that the film has peeled off above this layer.

Acknowledgment. This work was supported by the Deutsche Forschungsgemeinschaft as part of SFB 463, "Rare earth transition metal compounds: structure, magnetism and transport". G.H.C. is grateful for the financial support of the Alexander von Humboldt Foundation. We thank Prof. H. Lichte and Dr. M. Lehmann for assistance with HREM and H. Müller for preparation of the TEM samples.

CM050006T